Progress In Electromagnetics Research, PIER 81, 291–302, 2008

MULTILEVEL FAST MULTIPOLE ALGORITHM FOR RADIATION CHARACTERISTICS OF SHIPBORNE ANTENNAS ABOVE SEAWATER

X. W. Zhao, C. H. Liang, and L. Liang

National Key Laboratory of Antennas and Microwave Technology
Xidian University
Xi'an, Shaanxi 710071, China

Abstract—Radiation characteristics of shipborne antennas above lossy half-space are studied using the multilevel fast multipole algorithm (MLFMA). The near terms in the MLFMA are evaluated by using the rigorous half-space dyadic Green's function, computed via the method of complex images. The far MLFMA interactions employ an approximate dyadic Green's function via a direct-radiation term plus a single real image, with the image amplitude characterized by the polarization-dependent Fresnel reflection coefficient. Finally, radiation patterns of an ultra-shortwave antenna mounted on a realistic 3-D ship over seawater are presented and compared with a rigorous method-of-moments (MoM) solution.

1. INTRODUCTION

On electrically large ship-platforms, more and more antennas are used for different purposes. The platforms degrade the performance of these platform-mounted antennas. On the other hand, the environment (such as seawater) also affects the properties of the antennas. In order to simulate accurately the radiation characteristics of the shipborne antennas, we have to consider both the platforms and seawater (Fig. 1).

Electromagnetic scattering and radiating from targets in half-space has constituted a problem of long-term interest. Considering numerical modeling of such problems, there has been interest in method of moments (MoM) [1–3], finite-element method (FEM) [4] and finite difference time domain method (FDTD) [5, 6]. The MoM, FEM and FDTD algorithms can handle such targets in principle, but memory requirements and computation time become excessive. The high-frequency asymptotic techniques (e.g., PO, GTD, and UTD) [7, 8]

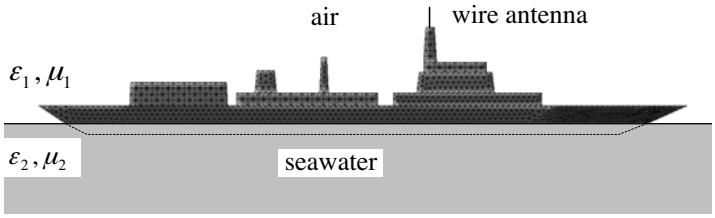

Figure 1. Cross section through shipborne antenna model over seawater.

can handle the large platforms, however they are not applicable or are difficult to implement to the half-space problems.

In [9–11], Geng and colleagues developed an approximate means of handling the dyadic half-space Green's function, with application to the fast multipole method (FMM) and the multilevel fast multipole algorithm (MLFMA), which were originally developed for targets in free space [12–22]. In their works, the near MLFMA terms are evaluated via the use of the exact dyadic Green's function, the latter evaluated efficiently via the complex-image technique [23]. The far terms, evaluated efficiently via the clustering algorithm, employ the asymptotic form of the dyadic Green's function. As elucidated further in the following, each component of the approximate Green's function is expressed in terms of the direct-radiation term plus radiation from an image source in real space [9–11]. The former accounts for the radiation of currents into the medium in which it resides, while the latter accounts for interactions with the half-space interface. The computational complexity of $O(N \log N)$, both in RAM and CPU (per iteration), remains unchanged compared to the free-space version [11]. However, Geng only applied the half-space FMM/MLFMA to scattering problems.

In this paper, the half-space MLFMA is applied to analysis of the radiation properties of shipborne antennas above seawater. A rigorous method of moments (MoM) [24] is achieved to validate the formula and the algorithm. Finally the radiation patterns for an ultra-shortwave antenna mounted on a full-scale ship model are obtained and discussed.

2. THEORY

2.1. Integral Equation and Half-space MoM Formulation

For solving the problem of scattering from an arbitrarily shaped 3-D, perfectly electric conducting (PEC) target situated above (i.e., target

in layer $i = 1$) or buried (i.e., target in layer $i = 2$) in a lossy half space (Fig. 1), we utilize the CFIE [14]

$$\hat{\boldsymbol{t}} \cdot \left[\alpha \boldsymbol{E}^{inc}(\boldsymbol{r}) + \eta_i(1-\alpha)\hat{\boldsymbol{n}} \times \boldsymbol{H}^{inc}(\boldsymbol{r})\right]\big|_{\boldsymbol{r}\in S} =$$
$$\alpha\hat{\boldsymbol{t}} \cdot \left[-\alpha \boldsymbol{E}^{scat}(\boldsymbol{r}) + \eta_i(1-\alpha)\boldsymbol{J}_s(\boldsymbol{r}) - \eta_i(1-\alpha)\hat{\boldsymbol{n}} \times \boldsymbol{H}^{scat}\left(\boldsymbol{r} \in S^+\right)\right] \quad (1)$$

with the scattered fields (inside half space i, in which the target is located) given by [1]

$$\begin{aligned}
\boldsymbol{E}^{scat}(\boldsymbol{r}) &= -j\omega\mu_i \left[\bar{\boldsymbol{I}} + \frac{\nabla\nabla}{k_i^2}\right] \cdot \iint\limits_{\boldsymbol{r}'\in S} \bar{\boldsymbol{G}}_{Aii}(\boldsymbol{r}, \boldsymbol{r}') \cdot \boldsymbol{J}(\boldsymbol{r}')\, dS' \\
&= -j\omega\mu_i \iint\limits_{\boldsymbol{r}'\in S} \bar{\boldsymbol{K}}_{Aii}(\boldsymbol{r}, \boldsymbol{r}') \cdot \boldsymbol{J}(\boldsymbol{r}')\, dS' \\
&\quad + \frac{\nabla}{j\omega\varepsilon_i} \iint\limits_{\boldsymbol{r}'\in S} K^{ii}_{\phi e}(\boldsymbol{r}, \boldsymbol{r}')\, \nabla' \cdot \boldsymbol{J}(\boldsymbol{r}')\, dS' \qquad (2a) \\
\boldsymbol{H}^{scat}(\boldsymbol{r}) &= \nabla \times \iint\limits_{\boldsymbol{r}'\in S} \bar{\boldsymbol{G}}_{Aii}(\boldsymbol{r}, \boldsymbol{r}') \cdot \boldsymbol{J}(\boldsymbol{r}')\, dS'. \qquad (2b)
\end{aligned}$$

The unit vectors $\hat{\boldsymbol{n}}$ and $\hat{\boldsymbol{t}}$ are perpendicular and tangential to the scatterer surface, respectively, $\boldsymbol{r}$ is on and $\boldsymbol{r} \in S^+$ is an infinitesimal distance outside the (closed) target surface. $\varepsilon_i = \varepsilon_i' - j\sigma_i/\omega$, μ_i, and k_i represent (in general complex) the permittivity, permeability, and wavenumber of the medium in which the target resides, and ω is the angular frequency (with a time dependence $\exp j\omega t$ assumed and suppressed). Details on the Green's function dyadics $\bar{\boldsymbol{G}}_{Aii}$ and $\bar{\boldsymbol{K}}_{Aii}$, as well as the scalar Green's function $K^{ii}_{\phi e}$ have been given by Michalski and Zheng in [1], where we use their formulation C. The CFIE in (1) is valid for a more general layered medium [1], but here we only consider the half-space problem for simplicity.

For near interactions (MoM part of the MLFMA), the evaluation of the impedance matrix elements, including the proper handling of self-term singularities and near singularity extraction, is done similar to the MoM literature [25]. The dyadic half-space Green's function is evaluated rigorously using the method of discrete complex images [23], thereby avoiding direct numerical evaluation of Sommerfeld integrals [1]. Impedance matrix elements representing these near interactions are stored in a sparse matrix called $[\boldsymbol{Z}^{near}]$. The method of complex images and explicit equations for the MoM impedance matrix elements can be found in literatures [1, 23], and therefore, we do not repeat the details.

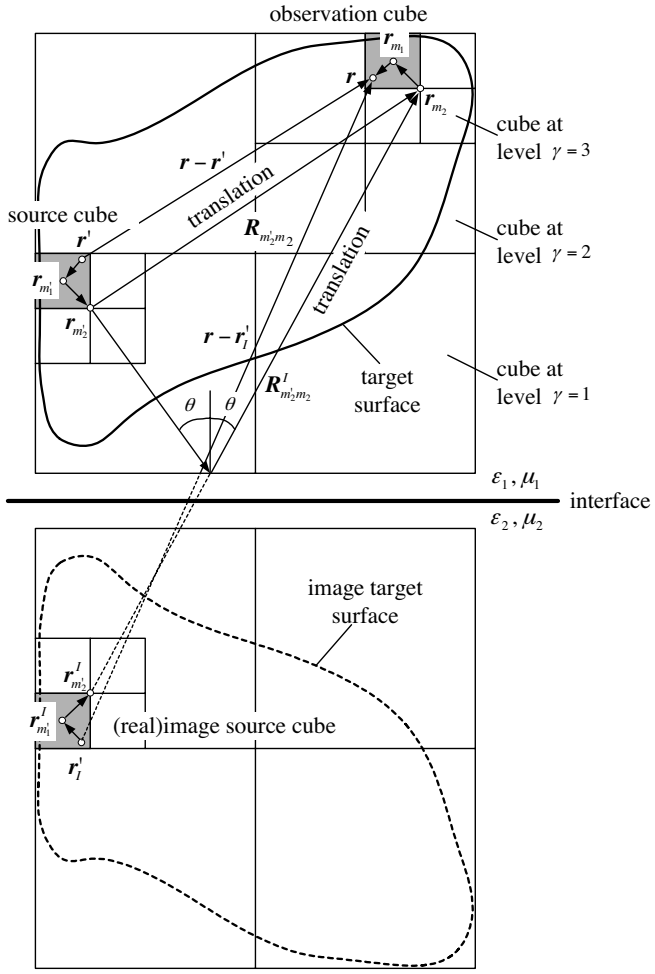

Figure 2. Cross section through multi-level clustering geometry in 3-D half-space MLFMA.

2.2. Free-space and Half-space MLFMA

The half-space dyadic Green's function can be split into a term $\bar{\boldsymbol{I}} g_i$ representing the "direct" radiation between source and observation point (as in free space, but using in general a complex wave number k_i) and a remaining dyadic $\Delta\bar{\boldsymbol{G}}_{Aii}$ accounting for interactions with the

interface (i.e., here Δ is not an operator) [9–11].

$$\bar{\boldsymbol{G}}_{Aii}\left(\boldsymbol{r},\boldsymbol{r'}\right)=\bar{\boldsymbol{I}}g_i\left(\boldsymbol{r},\boldsymbol{r'}\right)+\Delta\bar{\boldsymbol{G}}_{Aii}\left(\boldsymbol{r},\boldsymbol{r'}\right)=\bar{\boldsymbol{I}}\frac{e^{-jk_i|\boldsymbol{r}-\boldsymbol{r'}|}}{4\pi\left|\boldsymbol{r}-\boldsymbol{r'}\right|}+\Delta\bar{\boldsymbol{G}}_{Aii}\left(\boldsymbol{r},\boldsymbol{r'}\right) \tag{3}$$

While the dyadic $\Delta\bar{\boldsymbol{G}}_{Aii}$ needs some further investigation (see below), the *free-space* FMM [12, 13] or MLFMA [14] can be applied to the "direct" term, with only minor changes due to the (in general) lossy background. The *free-space* FMM and MLFMA are based on the addition theorem [12], leading to the (propagating) plane wave representation [12]

$$\begin{aligned} g_i\left(\boldsymbol{r},\boldsymbol{r'}\right) &= \frac{e^{-jk_i|\boldsymbol{r}-\boldsymbol{r'}|}}{4\pi\left|\boldsymbol{r}-\boldsymbol{r'}\right|} \\ &\approx \frac{-jk_i}{(4\pi)^2}\iint\limits_{4\pi} e^{-jk_i\hat{\boldsymbol{k}}\cdot(\boldsymbol{r}-\boldsymbol{r}_m)}T_L\left(k_iR_{m'm},\hat{\boldsymbol{k}}\cdot\hat{\boldsymbol{R}}_{m'm}\right) \\ &\quad \cdot e^{+jk_i\hat{\boldsymbol{k}}\cdot(\boldsymbol{r'}-\boldsymbol{r}_{m'})}d^2\hat{\boldsymbol{k}} \end{aligned} \tag{4a}$$

$$T_L\left(k_iR_{m'm},\hat{\boldsymbol{k}}\cdot\hat{\boldsymbol{R}}_{m'm}\right)=\sum_{l=0}^{L}(-j)^l(2l+1)h_l^{(2)}(k_iR_{m'm})P_l\left(\hat{\boldsymbol{k}}\cdot\hat{\boldsymbol{R}}_{m'm}\right) \tag{4b}$$

$$\hat{\boldsymbol{R}}_{m'm}=\boldsymbol{R}_{m'm}/R_{m'm}=\boldsymbol{R}_{m'm}/\sqrt{\boldsymbol{R}_{m'm}\cdot\boldsymbol{R}_{m'm}} \tag{4c}$$

of the scalar Green's function. The distance vector $\boldsymbol{R}=\boldsymbol{r}-\boldsymbol{r'}$ has been subdivided into a vector from the source point $\boldsymbol{r'}$ to the center $\boldsymbol{r'}_m$ of a "source group", a vector from an "observation group" center $\boldsymbol{r}_m$ to the observation point $\boldsymbol{r}$, and a vector connecting the group centers $\boldsymbol{R}_{m'm}$ (Fig. 1, where in this Section 2.2, we write $m'=m'_\gamma$, $m=m_\gamma$, and $\boldsymbol{R}_{m'm}=\boldsymbol{R}_{m'_\gamma m_\gamma}$ for simplification)

$$\boldsymbol{R}=\boldsymbol{r}-\boldsymbol{r'}=(\boldsymbol{r}-\boldsymbol{r}_m)+\boldsymbol{R}_{m'm}-\left(\boldsymbol{r'}-\boldsymbol{r}'_m\right)=\boldsymbol{R}_{m'm}+\boldsymbol{d}. \tag{5}$$

Using the expansion (4), the elements of the *far* interaction impedance matrix (i.e., for $\boldsymbol{R}_{m'm}$ sufficiently large) in the context of a free-space scattering problem can be written as [14]

$$Z_{nn'}=\frac{\omega\mu_ik_i}{(4\pi)^2}\iint\limits_{4\pi}\boldsymbol{W}_{m\alpha}\left(\hat{k}\right)\cdot T_L\left(k_iR_{m'm},\hat{\boldsymbol{k}}\cdot\hat{\boldsymbol{R}}_{m'm}\right)\cdot\boldsymbol{B}_{m'\alpha'}\left(\hat{k}\right)d^2\hat{\boldsymbol{k}} \tag{6}$$

$$\boldsymbol{B}_{m'\alpha'}\left(\hat{\boldsymbol{k}}\right) = \left[\bar{\boldsymbol{I}} - \hat{\boldsymbol{k}}\hat{\boldsymbol{k}}\right] \cdot \iint\limits_{\boldsymbol{r'}\in S'_n} \boldsymbol{b}_{n'(m',\alpha')}\left(\boldsymbol{r'}\right) e^{+jk_i\hat{\boldsymbol{k}}\cdot(\boldsymbol{r'}-\boldsymbol{r}_{m'})} dS' \qquad (7)$$

$$\begin{aligned}\boldsymbol{W}_{m\alpha}\left(\hat{\boldsymbol{k}}\right) \;=\; & \alpha\left[\bar{\boldsymbol{I}} - \hat{\boldsymbol{k}}\hat{\boldsymbol{k}}\right] \cdot \iint\limits_{\boldsymbol{r}\in S_n} \boldsymbol{w}_{n(m,\alpha)}\left(\boldsymbol{r}\right) e^{-jk_i\hat{\boldsymbol{k}}\cdot(\boldsymbol{r}-\boldsymbol{r}_m)} dS' dS \\ & + (1-\alpha)\,\hat{\boldsymbol{k}} \times \iint\limits_{\boldsymbol{r}\in S_n} \hat{n} \times \boldsymbol{w}_{n(m,\alpha)}\left(\boldsymbol{r}\right) e^{-jk_i\hat{\boldsymbol{k}}\cdot(\boldsymbol{r}-\boldsymbol{r}_m)} dS \qquad (8)\end{aligned}$$

where (7) and (8) represent the far-field radiation pattern of the basis functions and weighting pattern of the testing functions, respectively.

For a half-space FMM/MLFMA, it is essential to include the effects of the far interface interactions. However, that the number of terms L required for convergence can be prohibitively large for general complex source points, undermining the efficiency of using (4) for far interface interactions in the context of the discrete complex-image technique [9–11].

An alternative (though approximate) formulation is described in the following. While the half-space dyadic Green's function is rigorously accounted for in the near interaction matrix, far interactions are often less sensitive to approximations in the Green's function [9–11]. The FMM has been successfully extended to the scattering from a PEC object above or buried in a half space by employing the asymptotic form of the Green's function [11] for far interactions. The asymptotic form of the Green's function is represented utilizing a single real image at $\left[\bar{\boldsymbol{I}} - 2\hat{z}\hat{z}\right] \cdot r'$ (assuming the interface at $z = 0$) with its polarization dependent magnitude given by the reflection dyadic [11]

$$\bar{\boldsymbol{R}}\left(\hat{\boldsymbol{k}}\right) = \hat{\boldsymbol{h}}\hat{\boldsymbol{h}}\overleftarrow{\Gamma}_i^{TE}\left(\hat{\boldsymbol{k}}\right) + \left[\bar{\boldsymbol{I}} - \hat{\boldsymbol{h}}\hat{\boldsymbol{h}}\right]\overleftarrow{\Gamma}_i^{TM}\left(\hat{\boldsymbol{k}}\right) \quad \text{with} \quad \hat{\boldsymbol{h}} = \frac{\hat{\boldsymbol{z}} \times \hat{\boldsymbol{k}}}{\left|\hat{\boldsymbol{z}} \times \hat{\boldsymbol{k}}\right|}. \qquad (9)$$

Since this far-field reflection coefficient approximation cannot account for surface waves, the MLFMA presented here is valid for targets situated entirely within a single source layer (not the general layered medium as in [1]).

Therefore, in addition to the accurate calculation of the half-space dyadic Green's function in the near interaction matrix $[\boldsymbol{Z}^{near}]$ (Section 2.1), the half-space MLFMA only requires the definition of a single set of real image sources (Fig. 1), which can be handled similarly to real sources. Generalizing the free-space MLFMA [14] to

a half-space MLFMA is now straightforward. Besides some additional operations in the matrix-vector product [11], the preprocessing stage has to include calculations of the translation operators

$$T_L\left(k_i R^I_{m'm}, \hat{\boldsymbol{k}}\cdot\hat{\boldsymbol{R}}^I_{m'm}\right)=\sum_{l=0}^{L}(-j)^l\,(2l+1)\,h_l^{(2)}\left(k_i R^I_{m'm}\right)P_l\left(\hat{\boldsymbol{k}}\cdot\hat{\boldsymbol{R}}^I_{m'm}\right) \tag{10}$$

between image cube and observation cube centers for all non-nearby cubes at all levels, as well as the Fourier transforms

$$\begin{aligned}\boldsymbol{B}^I_{m'\alpha'}\left(\hat{\boldsymbol{k}}\right) \;=\; & \left[\bar{\boldsymbol{I}}-\hat{\boldsymbol{k}}\hat{\boldsymbol{k}}\right]\cdot\iint\limits_{\boldsymbol{r'}\in S'_n}\left[\bar{\boldsymbol{I}}-2\hat{\boldsymbol{z}}\hat{\boldsymbol{z}}\right]\\ & \cdot\boldsymbol{b}_{n'(m',\alpha')}\left(\boldsymbol{r'}\right)\cdot e^{+jk_i\hat{\boldsymbol{k}}\cdot\left[\bar{\boldsymbol{I}}-2\hat{\boldsymbol{z}}\hat{\boldsymbol{z}}\right]\cdot\left(\boldsymbol{r'}-\boldsymbol{r}_{m'}\right)}dS'\end{aligned} \tag{11}$$

of the image expansion functions $\left[\bar{\boldsymbol{I}}-2\hat{z}\hat{z}\right]\cdot\boldsymbol{b}'_n\left(\boldsymbol{r'}\right)$, where $\boldsymbol{R}^I_{m'm}$ is a vector from the image source group center $\boldsymbol{r}^I_{m'}$ to the observation group center (Fig. 1), and the dyadic $\bar{\boldsymbol{I}}-2\hat{z}\hat{z}$ accounts for the relative orientation and location of the image expansion functions, respectively.

3. NUMERICAL RESULTS AND DISCUSSION

The algorithm code of this work is written in Fortran format and run on a PC (Pentium IV 2.8 GHz CPU and 2.0 GB Memory). The accuracy of the MLFMA for the target in this section is verified through comparison with results computed via a rigorous MoM algorithm [24]. The BiCGStab (l) combined with block-diagonal preconditioner is utilized as the solver in the MLFMA, and a direct (LU-decomposition) solver in the MoM solution.

Consider a ship situated over lossy seawater with $\varepsilon_r = 80$ and $\sigma = 1\,\mathrm{S/m}$, as shown in Fig. 3. The model is 153 m in length and 16.5 m in width. A 30-MHz $\lambda/4$ monopole antenna is positioned on the model as shown in Fig. 3. We consider delta-gap excitation at the surface-wire junction. The surface of the ship is represented by 7648 planar triangles (8 basis functions per wavelength), and the antenna is divided into 14 segments.

Figure 4 shows the effect of seawater on the patterns of shipborne antenna. In Fig. 4, FS is short for Free-Space, and HS for Half-Space. In xoz and yoz planes, only the patterns in $z > 0$ space are given for half-space results, because we are interested in the radiation properties in air. From comparison, it is observed that the free-space and half-space MLFMA results agree very well with the corresponding MoM

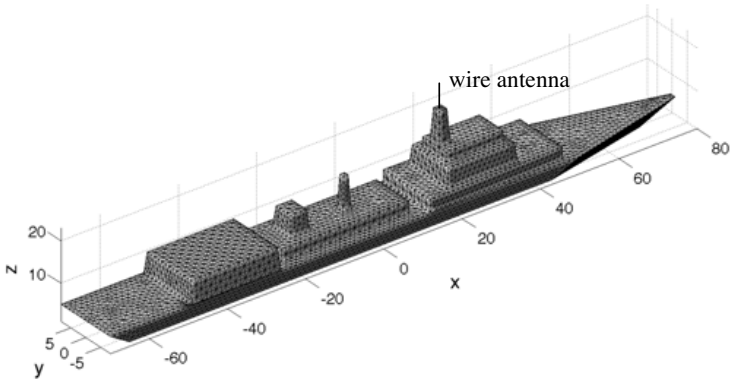

Figure 3. Shipborne antenna model over seawater.

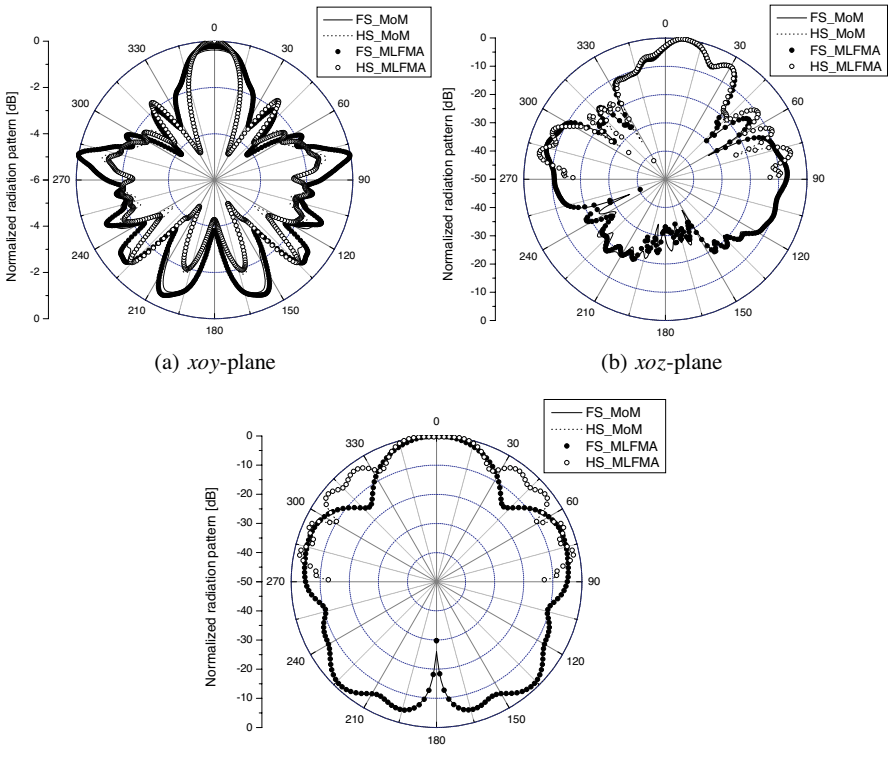

(a) *xoy*-plane

(b) *xoz*-plane

(c) *yoz*-plane

Figure 4. Normalized radiation patterns of shipborne antenna over seawater.

computed ones, respectively. Furthermore, the main lobe and side lobes of half-space radiation patterns are affected by the conduction coefficients and dielectric constants of seawater, especially in the range $30^\circ \leq \theta \leq 90^\circ$, compared to the free-space case. Therefore, both the ship platform and seawater should be considered in the analysis of shipborne antennas.

The memory requirement and the CPU time are listed in Table 1 (The convergence precision for BiCGStab ($l = 10$) is 10^{-3}). By comparison, it is observed that the free-space and half-space MLFMA achieve the same accuracy as the corresponding MoM version, respectively, but require far less simulation time and memory resources. With the above construct in Section 2.2, the real images introduce a new set of source clusters, and therefore, the half-space MLFMA requires slightly (about 43% in this example) more memory and about twice the computation time compared to the free-space version. However, The computational complexity of $O(N \log N)$, both in RAM and CPU (per iteration), remains unchanged compared to the free-space version [11]. The advantages of the MLFMA can be clearly seen when the electrical size of the object increases with the frequency.

Table 1. Performance comparison of MLFMA and MoM.

Algorithm	Memory (MB)	Time (sec)
free-space MoM	1003.6	2973.7
half-space MoM	1003.6	3905.2
free-space MLFMA	113.5	197.2
half-space MLFMA	162.8	345.6

We do not consider the portion under seawater for several reasons. First, as mentioned in Section 2.2, the half-space MLFMA presented here is invalid for targets crossing the half-space interface. Second, the portion under the ship broad has little effect on the radiation properties of the shipborne antennas [26]. Finally, meshing the portion over seawater leads to fewer unknowns compared to meshing the entire model.

4. CONCLUSIONS

Seawater effects have been considered for the analysis of electromagnetic radiations from shipborne antenna. From the results, it is clearly seen that the half-space radiation patterns are affected seriously by

the conduction coefficients and dielectric constants of seawater. The results presented here indicate that the seawater effects must be accounted for in many practical scenarios.

Within the context of non-nearby cluster computations, interaction with the half space is accounted for approximately via polarization-dependent images located at real spatial locations. In addition, the near interactions in the half-space MLFMA are treated via a rigorous analysis of the dyadic Green's function, here computed via the method of complex images. It has been found that such a rigorous analysis of the near interactions essential for generating accurate results.

REFERENCES

1. Michalski, K. A. and D. Zheng, "Electromagnetic scattering and radiation by surfaces of arbitrary shape in layered media, Parts I and II," *IEEE Trans. Antennas Propagat.*, Vol. 38, 335–352, March 1990.
2. Geng, N. and L. Carin, "Wideband electromagnetic scattering from a dielectric BOR buried in a layered lossy, dispersive medium," *IEEE Trans. Antennas Propagat.*, Vol. 47, 610–619, April 1999.
3. Su, D. Y., D. M. Fu, and D. Yu, "Genetic algorithm and method of moments for the design of PIFAS," *Progress In Electromagnetics Research Letters*, Vol. 1, 9–18, 2008.
4. Chang, H. S. and K. K. Mei, "Scattering of electromagnetic waves by buried and partly buried bodies of revolution," *IEEE Trans. Geosci. Remote Sensing*, Vol. 23, 596–605, 1985.
5. Bourgeois, J. M. and G. S. Smith, "A fully three-dimensional simulation of a ground-penetrating radar: FDTD theory compared with experiment," *IEEE Trans. Geosci. Remote Sensing*, Vol. 34, 36–44, January 1996.
6. Ding, W., Y. Zhang, P. Y. Zhu, and C. H. Liang, "Study on electromagnetic problems involving combinations of arbitrarily oriented thin-wire antennas and inhomogeneous dielectric objects with a hybrid MoM-FDTD method," *J. of Electromagn. Waves and Appl.*, Vol. 20, No. 11, 1519–1533, 2006.
7. Zhang, Y., X. W. Zhao, M. Chen, and C. H. Liang, "An efficient MPI virtual topology based parallel, iterative MoM-PO hybrid method on PC clusters," *J. of Electromagn. Waves and Appl.*, Vol. 20, No. 5, 661–676, 2006.
8. Chen, M., X. W. Zhao, Y. Zhang, and C. H. Liang, "Analysis

of antenna around NURBS surface with iterative MoM-PO technique," *J. of Electromagn. Waves and Appl.*, Vol. 20, No. 12, 1667–1680, 2006.

9. Geng, N., A. Sullivan, and L. Carin, "Fast multipole method for scattering from 3D PEC targets situated in a half-space environment," *Microwave Opt. Technol. Lett.*, Vol. 21, 399–405, 1999.
10. Geng, N., A. Sullivan, and L. Carin, "Fast multipole method for scattering from an arbitrary PEC target above or buried in a lossy half space," *IEEE Trans. Antennas Propagat.*, Vol. 49, 740–748, May 2001.
11. Geng, N., A. Sullivan, and L. Carin, "Multilevel fast-multipole algorithm for scattering from conducting targets above or embeded in a lossy half space," *IEEE Trans. Antennas Propagat.*, Vol. 38, 1561–1573, July 2000.
12. Coifman, R., V. Rokhlin, and S. Wandzura, "The fast multipole method for the wave equation: A pedestrian prescription," *IEEE Antennas Propagat Mag.*, Vol. 35, 7–12, June 1993.
13. Song, J. M. and W. C. Chew, "Fast multipole method solution using parametric geometry," *Microwave Opt. Technol. Lett.*, Vol. 7, 760–765, 1994.
14. Song, J. M. and W. C. Chew, "Multilevel fast multipole algorithm for solving combined field integral equations of electromagnetic scattering," *Microwave Opt. Technol. Lett.*, Vol. 10, 14–19, 1995.
15. Zhao, X. W., X. J. Dang, Y. Zhang, and C. H. Liang, "MLFMA analysis of waveguide arrays with narrow-wall slots," *J. of Electromagn. Waves and Appl.*, Vol. 21, No. 8, 1063–1078, 2007.
16. Zhao, X. W., X. J. Dang, Y. Zhang, and C. H. Liang, "The multilevel fast multipole algorithm for EMC analysis of multiple antennas on electrically large platforms," *Progress In Electromagnetics Research*, PIER 69, 161–176, 2007.
17. Wallen, H. and J. Sarvas, "Translation procedures for broadband MLFMA," *Progress In Electromagnetics Research*, PIER 55, 47–78, 2005.
18. Pan, X. M. and X. Q. Sheng, "A highly efficient parallel approach of multi-level fast multipole algorithm," *J. of Electromagn. Waves and Appl.*, Vol. 20, No. 8, 1081–1092, 2006.
19. Li, L. and Y. Xie, "Efficient algorithm for analyzing microstrip antennas using fast-multipole algorithm combined with fixed real-image simulated method," *J. of Electromagn. Waves and Appl.*, Vol. 20, No. 15, 2177–2188, 2006.

20. Ouyang, J., F. Yang, S. W. Yang, and Z. P. Nie, "Exact simulation method VSWIE+MLFMA for analysis radiation pattern of probe-feed conformal microstrip antennas and the application of synthesis radiation pattern of conformal array mounted on finite-length PEC circular cylinder with DES," *J. of Electromagn. Waves and Appl.*, Vol. 21, No. 14, 1995–2008, 2007.
21. Wang, P., Y. J. Xie, and R. Yang, "Novel pre-corrected multilevel fast multipole algorithm for electrical large radiation problem," *J. of Electromagn. Waves and Appl.*, Vol. 21, No. 13, 1733–1743, 2007.
22. Wang, P. and Y. J. Xie, "Scattering and radiation problem of surface/surface junction structure with multilevel fast multipole algorithm," *J. of Electromagn. Waves and Appl.*, Vol. 20, No. 15, 2189–2200, 2006.
23. Aksun, M. I., "A robust approach for the derivation of closed-form Green's functions," *IEEE Trans. Microwave Theory Tech.*, Vol. 44, 651–658, May 1996.
24. Zhang, Y., *Parallel Computation in Electromagnetics*, Xidian University Press, Xi'an, 2006 (in Chinese).
25. Hodges, R. E. and Y. Rahmat-Samii, "The evaluation of MFIE integrals with the use of vector triangle basis functions," *Microwave Opt. Technol. Lett.*, Vol. 14, 9–14, 1997.
26. Wang, M., "Prediction for the pattern of the antenna in a complex environment," Ph.D. dissertation, Xidian University, Xi'an, 2006 (in Chinese).